Progress In Electromagnetics Research M, Vol. 103, 129–140, 2021

A Compact CPW-Fed Triple-Band MIMO Antenna with Neutralization Line Decoupling for WLAN/WiMAX/5G Applications

Chengzhu Du[1, *], Zhuolin Zhao[1], Xun Wang[1], and Fuhui Yang[2]

Abstract—A compact CPW-fed triple-band Multiple Input Multiple Output (MIMO) antenna is designed for WLAN, WiMAX, and 5G applications in this article. Three resonant frequencies, including 2.4 GHz, 3.5 GHz, and 5.5 GHz are generated by two branches and a rectangle radiation patch. The proposed antenna comprises two antenna elements placed side by side with a meandering neutralization line (NL) inserted between the elements to realize decoupling. To analyze the performance, it is fabricated and experimented. The measured results reveal that it has three impedance bandwidths: 2.38–2.52 GHz (5.7%), 3.28–3.62 GHz (10.1%), and 5.05–6.77 GHz (29.1%) with the measured isolation up to 16 dB. Furthermore, the parameters of diversity performance like envelope correlation coefficient (ECC), diversity gain (DG), efficiency, gain, channel capacity loss (CCL), mean effective gain (MEG), and total active reflection coefficient (TARC) are also analyzed, and the results indicate that the proposed antenna is desirable for integration in WLAN/WiMAX/5G devices.

1. INTRODUCTION

In the context of the development and update of wireless communication technology, more communication data volume, faster rate of transmission, more reliable performance, and improved channel capacity are desired. The technology of multiple-input-multiple-output (MIMO) can help to fulfill these demands as it contains multiple transmitting and receiving antenna elements to handle a mass of data. Furthermore, mobile communication system has been developed to the fifth-generation (5G) with a higher transmission rate and more access devices. Among the spectral range of the 5G system, sub-6 GHz has drawn attention as it coincides with the frequency spectrum like WLAN, WiMAX, Wi-Fi, Bluetooth, etc. [1, 2].

Recently, many MIMO antennas with triple bands have been proposed [3–16]. The antennas with triple-band form without any isolation branches are reported in [3–7]. In [4], an inverted L-shaped slot and a meander line are introduced to achieve triple bands, and the elements are placed opposite to one another to realize decoupling and maintain the compactness. In [5], the antenna can operate in triple-bands by the patch etched with a U-slot, and the elements are arranged side by side with the mutual coupling decreasing to below −20 dB. In [6], an inverted L-shaped monopole and split ring resonators (SRRS) are used to realize triple-bands, and the antenna elements are arranged vertically to one another to exhibit an isolation more than 14 dB. However, these antennas [3–7] tend to be formed with a plain structure to generate triple-bands so that they can obtain an acceptable isolation without any isolators. In [8–10], it is proposed that stubs are used in these antennas to obtain enhanced isolation. In [8], an antenna uses three semicircles to generate three resonant frequencies. To enhance the isolation, two

Received 23 April 2021, Accepted 23 June 2021, Scheduled 14 July 2021
* Corresponding author: Chengzhu Du (duchengzhu@163.com).
[1] College of Electronics and Information Engineering, Shanghai University of Electric Power, Shanghai 200090, China. [2] CETC Shanghai Microwave Communication Co., Ltd, Shanghai, China.

elements are placed side by side with an interdigital capacitor (IDC) located between them. In [9], an antenna is designed with a tri-arm monopole to work within three bands, and the isolation better than 20 dB is achieved by integrating a stub on the background plane between elements and a stub added in the feed line. These MIMO antennas are generally formed with multiple stubs to achieve multiple-bands, resulting in the current coupling through the stubs. So, they need to introduce a new path to diminish the mutual coupling. It is reported in [11, 12] that these MIMO antennas with triple-bands use a defected ground structure (DGS) to block the current flowing through the ground to improve the isolation. In [13], an antenna combines a T-shaped slot on the ground plane and a meander-line connecting to the slot to realize decoupling at the highest and lowest frequency bands. It is reported in [14–16] that a neutralization line (NL) is used to achieve an enhanced isolation, which can realize decoupling and compactness at the same time. Based on these previous studies on triple-band MIMO antennas, it can be concluded that the decoupling for a triple-band MIMO antenna is a challenge task.

In this article, a triple-band MIMO antenna with two elements is designed, then fabricated and tested. The feeding method of it is coplanar waveguide (CPW), helping to obtain a better impedance match. To improve the isolation, we use the meandering NL placed in the gap between the two antenna elements. The measured results show that the antenna has an operating bandwidth covering 2.38–2.52 GHz, 3.28–3.63 GHz, and 5.05–6.77 GHz, fulfilling the radio spectrum including WLAN (2.4–2.48/5.15–5.35/5.725–5.825 GHz), WiMAX (5.25–5.85 GHz), and 5G (3.3–3.6 GHz) with the isolation better than 18.2 dB, 16.3 dB, and 17.1 dB, respectively. In addition, diversity performance has been analyzed, including ECC (< 0.005), DG (> 9.99), CCL (< 0.4 bits/s/Hz), the difference of MEG (< 2 dB), and TARC (< -10 dB) within working bands, indicating that the proposed antenna is desirable for the usage of WLAN, WiMAX, and 5G communications.

In the following sections of this paper, we detail the antenna geometry, antenna design process, analysis on the NL, measured results, and the analysis on diversity performance.

2. ANTENNA DESIGN

2.1. Antenna Geometry

The geometry of the proposed antenna and a photo of the fabricated antenna are shown in Figures 1(a) and (b), respectively. The antenna is printed on an FR4 dielectric substrate with an overall size of 56 mm $*$ 30 mm $*$ 1.6 mm, relative dielectric constant of 4.4, and loss tangent of 0.02. It comprises two radiation elements placed side by side and an NL connecting between the elements to decrease the undesirable mutual coupling. The three resonant frequencies are implemented by the radiating elements containing a rectangular patch, an L-shaped branch extending from the patch, and a strip

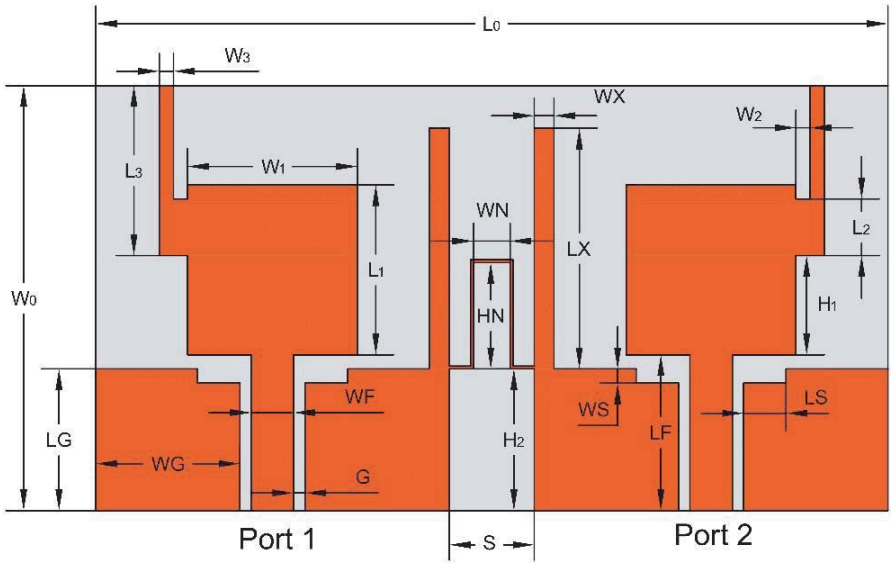

(a)

(b)

Figure 1. (a) Geometry of the proposed antenna and (b) photo of the fabricated antenna with the dimensions (in mm): $L_0 = 56\,\text{mm}$, $W_0 = 30\,\text{mm}$, $LG = 10\,\text{mm}$, $WG = 10.8\,\text{mm}$, $G = 0.2\,\text{mm}$, $WF = 3\,\text{mm}$, $L_1 = 12\,\text{mm}$, $W_1 = 12\,\text{mm}$, $W_2 = 1\,\text{mm}$, $L_2 = 4\,\text{mm}$, $WS = 1\,\text{mm}$, $LS = 3\,\text{mm}$, $W_3 = 1\,\text{mm}$, $L_3 = 12\,\text{mm}$, $H_1 = 7\,\text{mm}$, $WX = 1.4\,\text{mm}$, $LX = 17\,\text{mm}$, $WN = 3\,\text{mm}$, $HN = 10\,\text{mm}$, $H_2 = 10\,\text{mm}$, $LF = 11\,\text{mm}$, $S = 6\,\text{mm}$.

stretching from the ground plane to generate the resonant frequencies of 5.5 GHz, 3.5 GHz, and 2.4 GHz, respectively. The antenna elements are fed by coplanar waveguide (CPW) with the gap between them keeping at 6 mm. The ground plane is etched with a rectangular slot to improve impedance bandwidth at the 5.5-GHz band.

2.2. Antenna Design Process

Figure 2 presents the antenna design process. It steps from Ant A, through Ant B to Ant C. During the design process, the software ANSYS HFSS is employed to implement the simulation and optimization of the antenna. In Figures 3(a) and (b), simulated S_{11} and S_{21} are presented, respectively.

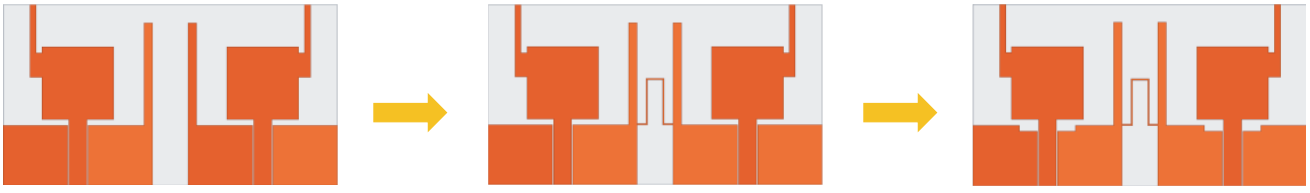

Figure 2. Process of the antenna design.

The proposed MIMO antenna is originated from the triple-band antenna element with a rectangle monopole, a strip extending from the ground plane, and an L-shaped branch connecting to the rectangle monopole, which are responsible for 5.5 GHz band, 2.4 GHz band, and 3.5 GHz bands, respectively. The lengths of the strip from the ground plane and the L-shaped branch are close to a quarter of dielectric wavelength. The dimensions of the rectangle monopole (L1 and W1) can be obtained by the basic rectangle antenna equation [19, 20] as follows:

$$W = \frac{c}{2f}\sqrt{\frac{\varepsilon_r+1}{2}} \tag{1}$$

$$L = \frac{c}{2f\sqrt{\varepsilon_r}} - 2\Delta L, \quad \Delta L = 0.412 \frac{(\varepsilon_r + 0.3)\left(\frac{W}{h} + 0.264\right)}{(\varepsilon_r - 0.258)\left(\frac{W}{h} + 0.8\right)} h \tag{2}$$

where W and L represent the length and width of the rectangle monopole; c is the light speed in vacuum; f is the resonant frequency; and ε_{eff} is the effective relative permittivity.

When Ant A is designed with the two the triple-band antenna elements placed side by side without any decoupling structure, the operating band ($S_{11} < -10$ dB) covers 2.4–2.5 GHz, 3.2–3.8 GHz, and 5.2–10.0 GHz while the value of S_{21} at 2.4 GHz is only about -10 dB which indicates the worse isolation at 2.4-GHz band. Then, a meandering NL is introduced between elements in Ant B. From Figure 3, it can be obtained that the value of S_{21} drops to lower than -20 dB at 2.4-GHz band, showing that the added NL can build a new current path to prevent the current from flowing to the other elements. However, in both Ant A and Ant B, the performance of impedance match at a 5.5-GHz band is not good enough. In Ant C, a rectangular slot is etched on the ground plane to reduce the proximity effects. The value of S_{11} at 5.5-GHz band drops to below -18 dB, confirming that the defected structure has an effective influence on extending the operating bandwidth especially at 5.5-GHz band.

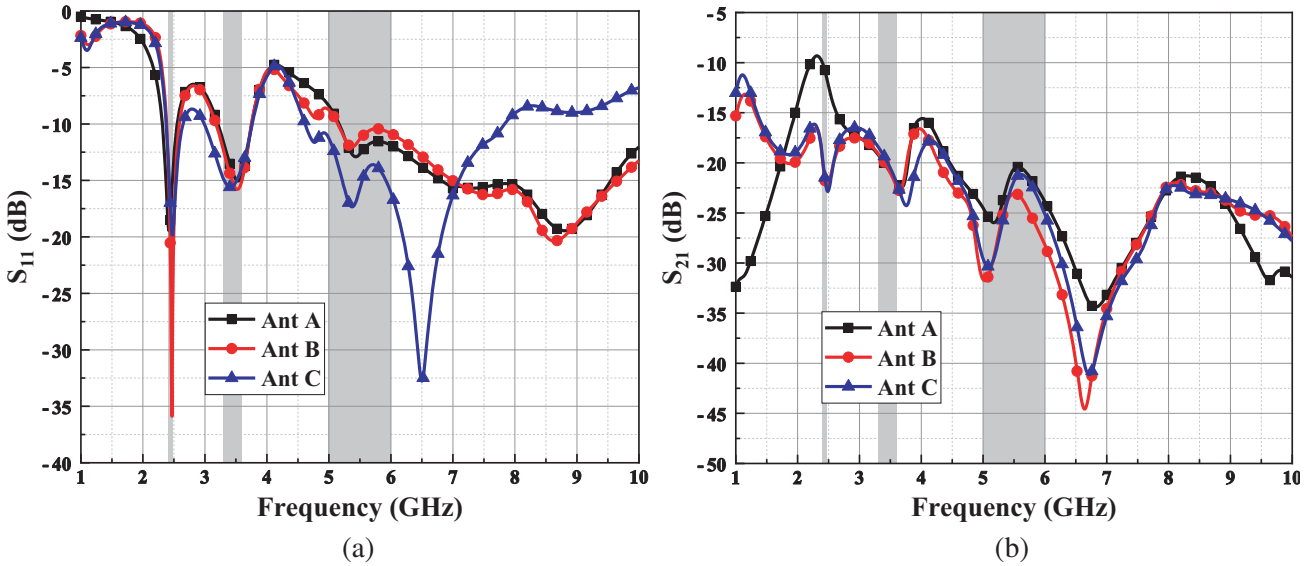

Figure 3. Simulated (a) S_{11} and (b) S_{21} of Ant A, Ant B and Ant C.

3. ANALYSIS OF THE ISOLATION STRUCTURE

To deeply investigate the effect of the NL introduced between elements, we do an analysis on the parametric study, surface current, and E-field distribution.

Figure 4 shows the S-parameters of the variation of HN, denoting the length of the NL. As the length of NL increases, the isolation at 2.4-GHz band is improved, and the operating bandwidth is changed little. Figure 5 plots the S-parameters with the variation of H_2, representing the height of NL. The results indicate that if the NL is located higher, the value of S_{21} would be better at 2.4-GHz band. Then, by adjusting and optimizing the values of HN and H_2, an enhanced isolation is obtained with $HN = 10$ mm and $H_2 = 10$ mm.

Figures 6(a) and (b) exhibit the surface current distribution and E-field distribution, respectively, by connecting Port 1 to excitation source and matching Port 2 with 50-Ω load. In Figure 6(a), it can be observed that when the NL is added in the middle of these two elements, the surface current flows along the path of the NL instead of flowing into Port 2. So, it is clear that the current density is diminished

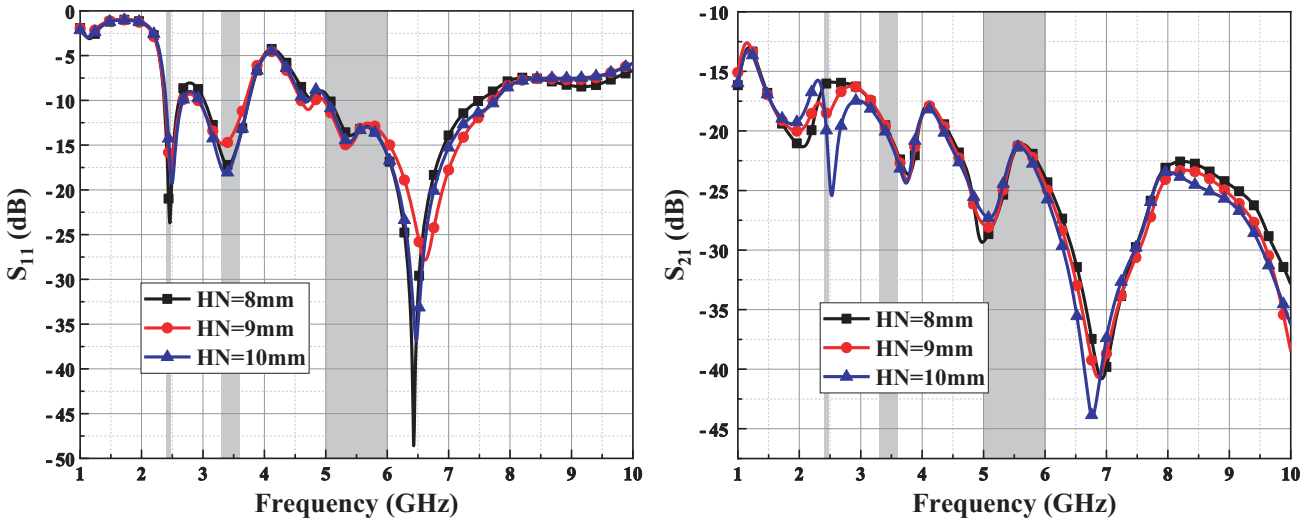

Figure 4. Simulated (a) S_{11} and (b) S_{21} of the antenna with variation of HN.

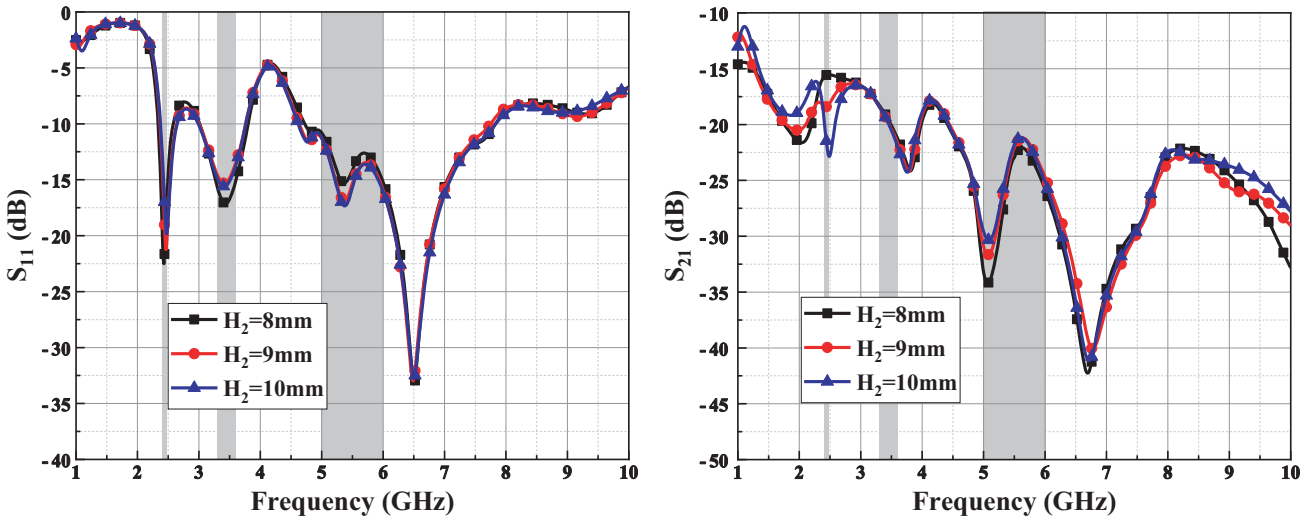

Figure 5. Simulated (a) S_{11} and (b) S_{21} of the antenna with the variation of H_2.

at Port 2, compared with the surface distribution of Ant A without any isolation structure. Similarly, the electric field distribution indicates the effective reduction after the introduction of the NL.

4. ANTENNA PERFORMANCE

4.1. Experimental Verification

4.1.1. S-Parameters

To verify the performance, the proposed antenna is fabricated, and then experimented by Agilent PNA-L N5230A Network Analyzer. The measurement method is to connect Port 1 to excitation source and Port 2 to 50-Ω load. Figure 7 shows the simulated and measured S_{11} and S_{21} of the proposed

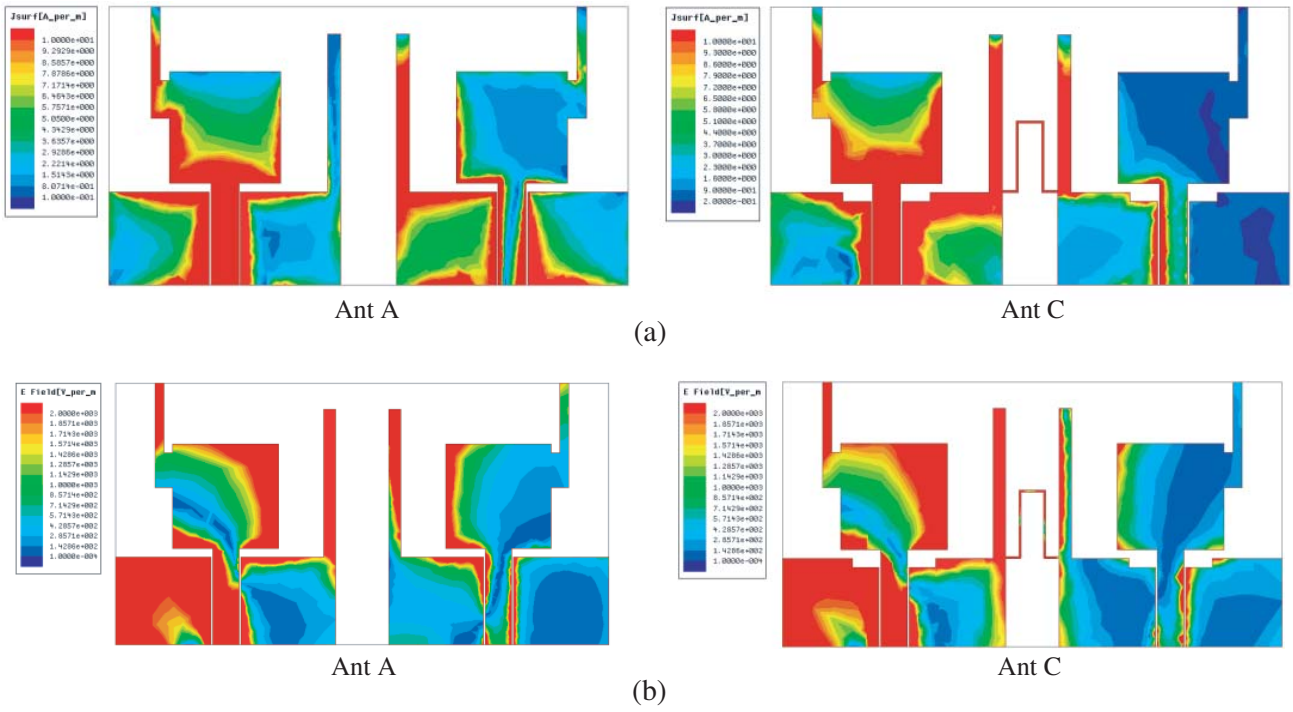

Figure 6. Simulated (a) surface current distribution and (b) E-field distribution of Ant A and Ant C at 2.4 GHz.

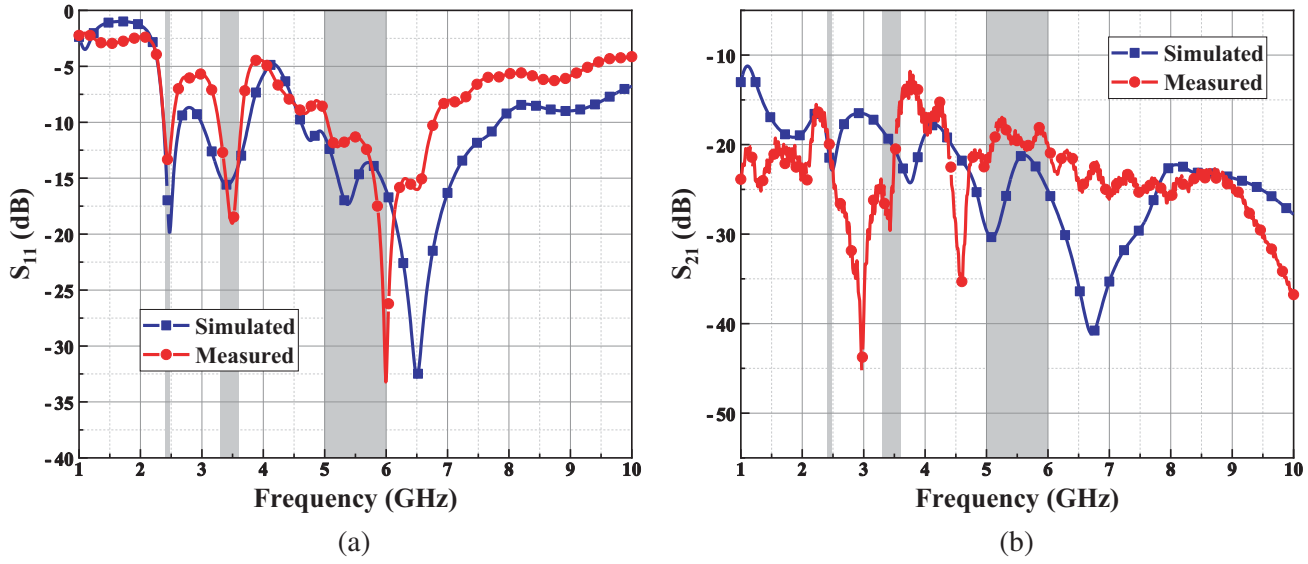

Figure 7. Simulated and measured (a) S_{11} and (b) S_{21} of the proposed MIMO antenna.

antenna, showing that the measured S_{11} covers triple-bands within 2.38–2.52 GHz, 3.28–3.63 GHz, and 5.05–6.77 GHz ($S_{11} < -10$ dB) with the fractional bandwidths of 5.7%, 10.1%, and 29.1%, which correspond to the simulated results. The measured isolations between elements is better than 18 dB, 16 dBs and 17 dB within 2.4 GHz, 3.5 GHz, and 5.5 GHz, respectively. In comparison between simulated and measured results, there exists a little difference which can be contributed to the loss of SMA connector, the error during the fabrication, and the uncertainty of measurement environment.

4.1.2. Radiation Pattern

To investigate the radiation mechanism, both the normalized radiation patterns in E-plane (XZ plane) and H-plane (YZ plane) have been simulated and measured at 2.4 GHz, 3.5 GHz, and 5.5 GHz as shown in Figure 8. From Figure 8, it can be observed that radiation patterns in these three resonant frequencies appear omnidirectional, and the level of cross-polarization is generally inferior to that of co-polarization at these frequencies except a few degrees. On account of the symmetrical structure, we only test the radiation patterns with Port 1 excited and Port 2 matched load.

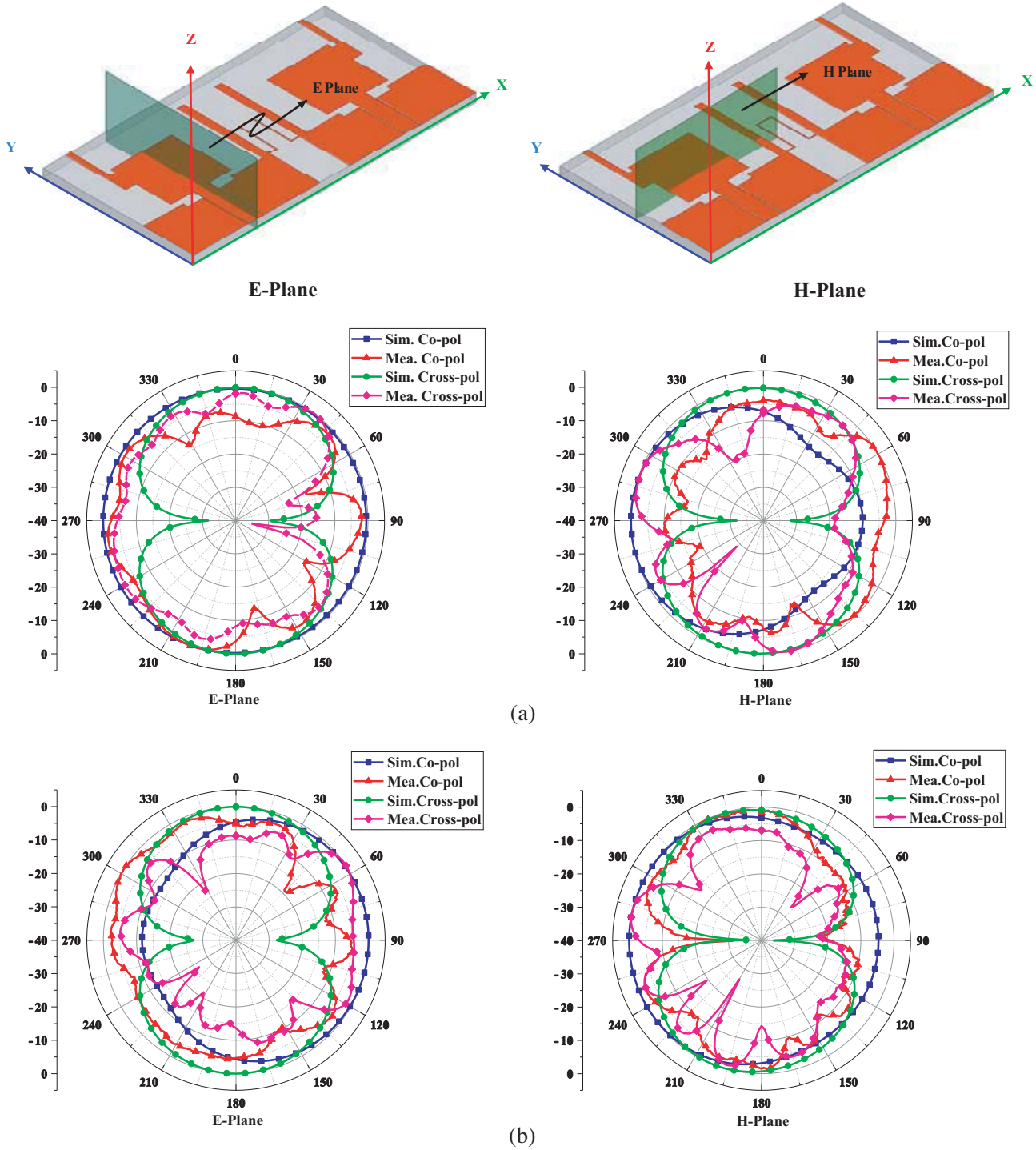

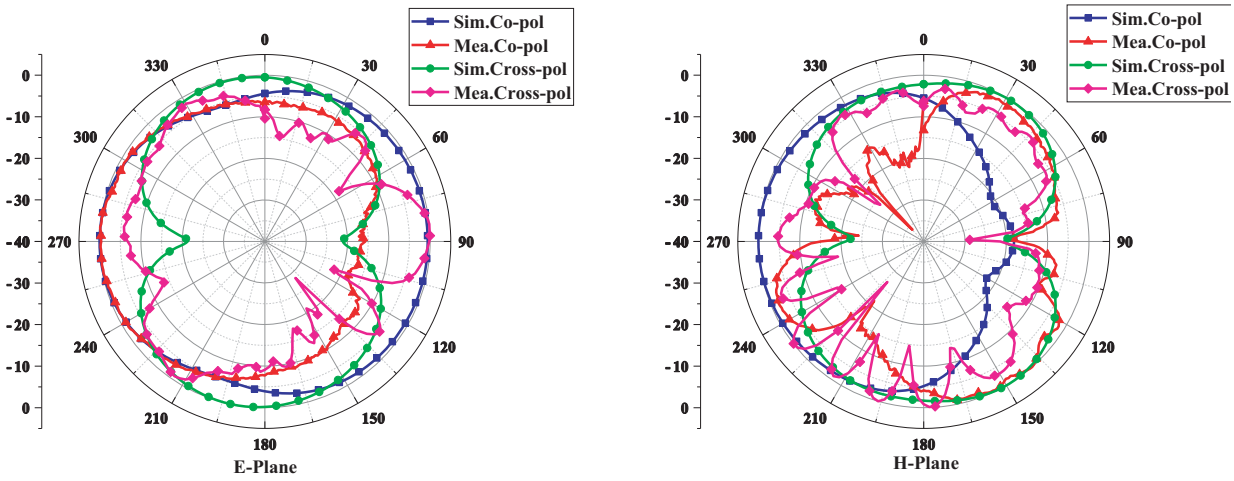

(c)

Figure 8. Simulated and measured radiation patterns in E-plane (XZ plane) and H-plane (YZ plane) at (a) 2.4 GHz, (b) 3.5 GHz and (c) 5.5 GHz.

4.1.3. Gain and Efficiency

Figure 9 exhibits the simulated and measured results of peak gain covering 2.0 GHz–6.0 GHz. Among them, the measured average peak gain is around 1.5, 0.5, and 4.5 dB for 2.4, 3.5, and 5.5 GHz bands, respectively. In addition, the simulated gain shows a higher level than the measured gain, which can be attributed to the difference of measurement and the uncertainty of the environment.

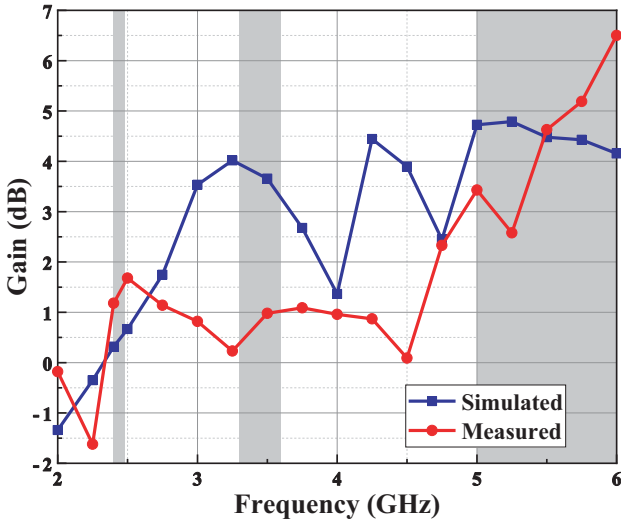

Figure 9. Simulated and measured gain.

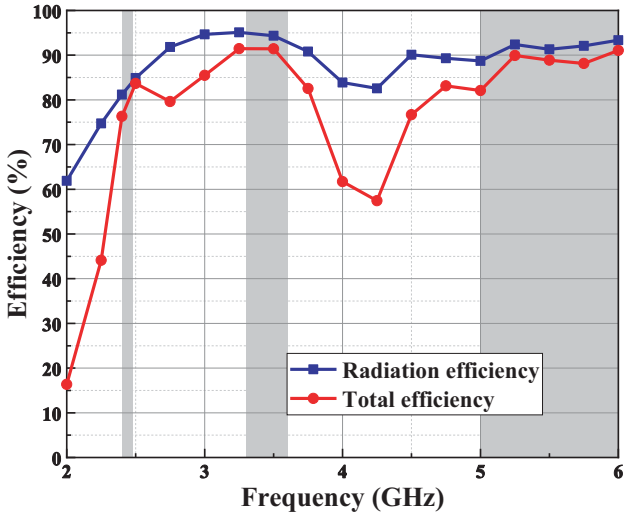

Figure 10. Radiation and total efficiency.

As an important parameter, efficiency is employed to assess the performance of the antenna. The radiation efficiency and total efficiency are plotted in Figure 10. In the curves, it can be seen that the radiation efficiencies are around 82.5%, 95%, and 90% in 2.4, 3.5, and 5.5 GHz bands, respectively, and the total efficiencies are around 80%, 90%, and 90% for the three bands. Moreover, the overall level of radiation efficiency is superior to that of total efficiency.

4.2. Diversity Performance

To have a further analysis of the antenna, some valuable diversity parameters should be taken into consideration like envelope correlation coefficient (ECC), diversity gain (DG), channel capacity loss (CCL), mean effective gain (MEG), and total active reflection coefficient (TARC), which are presented in the following sections.

4.2.1. Envelope Correlation Coefficient and Diversity Gain

The parameter ECC describes the degree of correlation between antenna elements when they are placed in a limited area, resulting in the degradation of the isolation and performance of antenna. Considering that the MIMO antenna proposed in this paper has two elements, we can compute ECC by the following equation [17]:

$$ECC = \frac{\left|S_{11}^{*}S_{12} + S_{21}^{*}S_{22}\right|^{2}}{\left(1 - \left|S_{11}\right|^{2} - \left|S_{21}\right|^{2}\right)\left(1 - \left|S_{22}\right|^{2} - \left|S_{12}\right|^{2}\right)} \tag{3}$$

Generally, the value of ECC less than 0.5 within operating bands can be allowed for practical use. It is shown in Figure 11, the curves of ECC, that both simulated and measured ECCs are less than 0.005, which is far beyond the requirement.

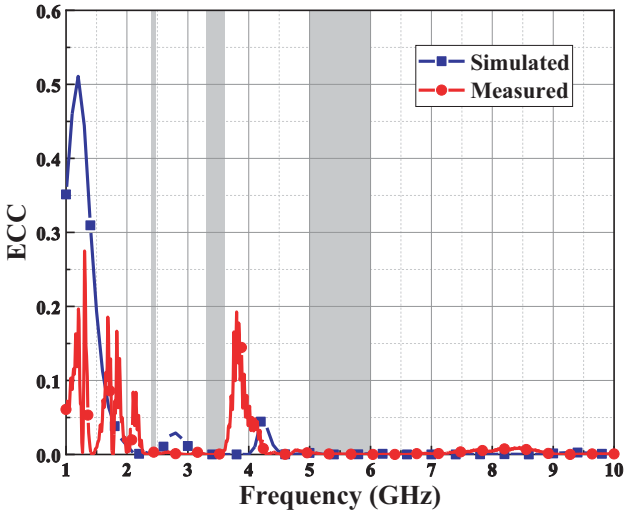

Figure 11. Simulated and measured ECC.

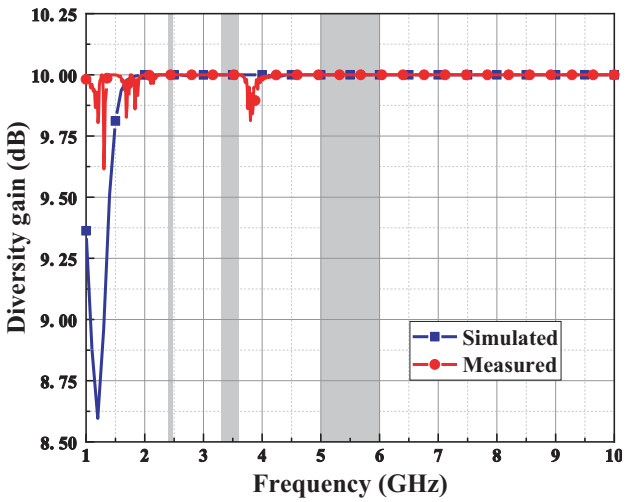

Figure 12. Simulated and measured DG.

Diversity gain is also used for analyzing the performance of MIMO antenna. We can calculate it by the equation below:

$$DG = 10\sqrt{1 - (ECC)^{2}} \tag{4}$$

Figure 12 shows the curves of DG ranging from 1.0 GHz to 10.0 GHz, presenting that the level of DG is better than 9.99.

4.2.2. Channel Capacity Loss and Mean Effective Gain

The parameter of channel capacity loss (CCL) describes how fast the constant message transmission rate can attain in communication system, and the CCL for MIMO antenna should maintain lower than 0.4 bits/s/Hz over working bands. We can calculate the value of CCL by the following equation [18]:

$$CCL = -\log_{2}\det\left(\Psi^{R}\right) \tag{5}$$

where $\Psi^R=\begin{bmatrix}\Psi_{11} & \Psi_{12}\\ \Psi_{21} & \Psi_{22}\end{bmatrix}$, $\Psi_{ii}=1-(|S_{ii}|^2+|S_{ij}|^2)$, $\Psi_{ij}=-(S_{ii}^*S_{ij}+S_{ji}^*S_{ij})$.

MEG defines how much the power is obtained by MIMO antenna when fading environment is considered. Generally, we compute the difference of MEG_i between two ports by using the following equation:

$$MEG_i=0.5\eta_{i,rad}=0.5\left(1-\sum_{j=1}^{M}|S_{ij}|^2\right) \tag{6}$$

$$|MEG_i-MEG_j|<3\,\mathrm{dB} \tag{7}$$

The computed CCL and MEG curves are plotted in Figure 13. In practice, the level of CCL should be below 0.4 bits/s/Hz, and the difference of MEG_i should be maintained lower than 3 dB. We can see from the figure that the CCL is below 0.4 bits/s/Hz over operating bands, and the difference between MEG_1 and MEG_2 is below 2 dB, which can indicate a good performance of the proposed antenna.

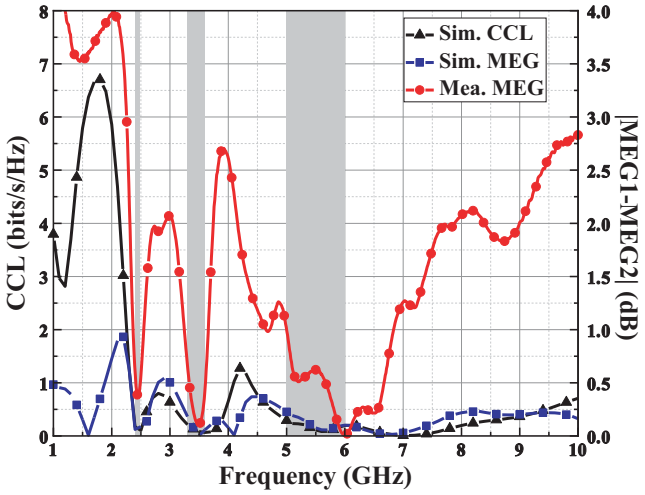

Figure 13. Simulated and measured CCL and MEG.

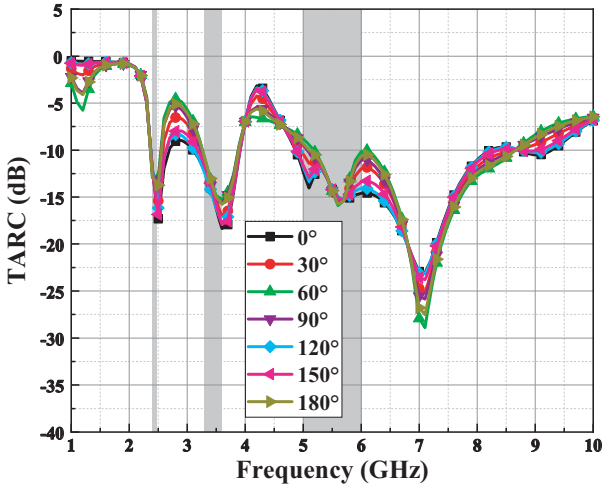

Figure 14. Simulated and measured TARC.

4.2.3. Total Active Reflection Coefficient

Total active reflection coefficient (TARC) is an important parameter to have a comprehensive evaluation of the frequency bandwidth and the extent of mutual coupling of MIMO antenna. We can calculate TARC by the following equation:

$$TARC=\frac{\sqrt{\left(|S_{11}+S_{12}e^{j\theta}|^2+|S_{21}+S_{22}e^{j\theta}|^2\right)}}{\sqrt{2}} \tag{8}$$

where θ represents the excitation phase angle. In this paper, we pick six phase angles: 0°, 30°, 60°, 120°, 150°, and 180° to analyze the characteristic of the proposed antenna. Figure 14 exhibits the curve of TARC ranging from 1 GHz to 10 GHz. It can be observed that TARC is below −10 dB over the operating bands, showing a stable characteristic and an allowable isolation of the MIMO antenna.

5. PERFORMANCE COMPARISON

Table 1 shows the comparison of the antenna in this paper with previous designs in terms of overall size, decoupling approach, feeding method, bandwidth, isolation, ECC, and DG. Compared with the

Table 1. Comparison of the proposed MIMO antenna with previous antennas.

Ref.	No. of ports	Antenna Size (mm)	Decoupling Approach	Feeding Method	Bandwidth (GHz)	Isolation (dB)	ECC	DG
[6]	4	$40 * 40$	Orthogonal	Microstrip	2.4, 3.45, 5.5	14	-	-
[9]	2	$38 * 37$	Ground stub	Microstrip	2.1–2.7, 3.29–3.67, 4.9–5.35	20	< 0.05	-
[12]	2	$45 * 25$	Defected ground structure	Microstrip	2.37–2.64, 3.39–3.58, 4.86–6.98	15, 23, 15	< 0.012	-
[14]	2	$49 * 48$	Neutralization line	Microstrip	2.24–2.45, 3.3–4, 5.6–5.75	18.2, 32.4, 24.3	< 0.02	> 9.9
Prop.	2	$56 * 30$	Neutralization line	CPW	2.38–2.52, 3.28–3.63, 5.05–6.77	18.2, 16.3, 17.1	< 0.005	> 9.99

previous antennas, the antenna in this paper shows a compact structure for the introduction of NL, a broader bandwidth in the design of triple-band MIMO antenna, easier integration for the feeding method of CPW feeder, an enhanced isolation in lower band, a low level of ECC, and a better level of DG, confirming the advantage of the proposed triple-band MIMO antenna.

6. CONCLUSION

A compact CPW-fed triple-band MIMO antenna is proposed in this article. According to the measured results, it can operate bandwidth covering 2.38–2.52, 3.28–3.63, and 5.05–6.77 GHz, which can meet the radio spectrum, including WLAN (2.4–2.48/5.15–5.35/5.725–5.825 GHz), WiMAX (5.25–5.85 GHz), and 5G (3.3–3.6 GHz). The introduction of an NL between elements successfully makes an improvement in the isolation, and the slot etched on the ground plane optimizes impedance match effectively. The measured isolations are better than 18.2 dB, 16.3 dB, and 17.1 dB within 2.4-GHz, 3.5-GHz, and 5.5-GHz bands, respectively. Moreover, the proposed antenna also possess a suitable ECC (< 0.005), DG (> 9.99), CCL (< 0.4 bits/s/Hz), the difference of MEG (< 2 dB), and TARC (< -10 dB), confirming that the proposed MIMO antenna is competent for WLAN/WiMAX/5G communications.

ACKNOWLEDGMENT

This work was supported by the National Natural Science Foundation of China under Grant No. 61371022.

REFERENCES

1. Sun, L. B., Y. Li, Z. J. Zhang, and Z. H. Feng, "Wideband 5G MIMO antenna with integrated orthogonal-mode dual-antenna pairs for metal-rimmed smartphones," *IEEE Trans. Antennas Propag.*, Vol. 68, No. 4, 2494–2503, 2020.
2. Bengtsson, E. L., F. Rusek, et al., "A simulation framework for multiple-antenna terminals in 5G massive MIMO systems," *IEEE Access*, Vol. 5, 26819–26831, 2017.

3. Islam, S. N., M. Kumar, et al., "Design of a compact triple band antenna with independent frequency tuning for MIMO applications," *Int. J. RF Microw. Comput. Aided Eng.*, Vol. 29, No. 3, e21620, 2019.
4. Kumar, M. and V. Nath, "Design and development of triple-band compact ACS-fed MIMO antenna for 2.4/3.5/5 GHz WLAN/WiMAX applications," *Analog Integrated Circuits and Signal Processing*, Vol. 103, No. 3, 461–470, 2020.
5. Liang, J. J., G. L. Huang, et al., "A triple-band antenna for MIMO WLAN applications," *Int. J. RF Microw. Comput. Aided Eng.*, Vol. 28, No. 5, e21251, 2018.
6. Rajeshkumar, V. and R. Rajkumar, "SRR loaded compact tri-band MIMO antenna for WLAN/WiMAX applications," *Progress In Electromagnetics Research Letters*, Vol. 95, 43–53, 2021.
7. Goud, J. R., N. K. Rao, and A. M. Prasad, "Design of triple band U-slot MIMO antenna for simultaneous uplink and downlink communications," *Progress In Electromagnetics Research C*, Vol. 106, 271–283, 2020.
8. Amit, K., A. Abdul, et al., "Design of triple-band MIMO antenna with one band-notched characteristic," *Progress In Electromagnetics Research C*, Vol. 86, 41–53, 2018.
9. Chaudhari, A. A. and R. K. Gupta, "A simple tri-band MIMO antenna using a single ground stub," *Progress In Electromagnetics Research C*, Vol. 86, 191–201, 2018.
10. Pasumarthi, S. R., J. B. Kamili, and M. P. Avala, "Design of tri-band MIMO antenna with improved isolation using DGS and Vias," *Wireless Personal Communications*, Vol. 110, No. 3, 1523–1532, 2020.
11. Niu, B. J. and J. H. Tan, "Compact tri-band MIMO antenna based on quarter-modeslotted substrate-integrated-waveguide cavity," *Int. J. RF Microw. Comput. Aided Eng.*, Vol. 30, No. 3, e22101, 2019.
12. Nandi, S. and A. Mohan, "CRLH unit cell loaded tri-band compact MIMO antenna for WLAN/WiMAX applications," *IEEE Antennas Wireless Propag. Lett.*, Vol. 16, 1816–1819, 2017.
13. Sun, J. S. and H. S. Fang, "Triple-band MIMO antenna for mobile wireless applications," *IEEE Antennas Wireless Propag. Lett.*, Vol. 15, 500–503, 2016.
14. Liu, R. P., X. An, et al., "Neutralization line decoupling tri-band multiple-input multiple-output antenna design," *IEEE Access*, Vol. 8, 27018–27026, 2020.
15. Biswas, A. K. and U. Chakraborty, "Investigation on decoupling of wide band wearable multiple-input multiple-output antenna elements using microstrip neutralization line," *Int. J. RF Microw. Comput. Aided Eng.*, Vol. 29, No. 7, e21723, 2019.
16. Saleh, A. M. and K. H. Sayidmarie, "Compact tri-band MIMO antenna with high port isolation for WLAN and WiMAX applications," *Loughborough Antennas & Propagation Conference (LAPC)*, 2016.
17. Du, C. Z. and Z. L. Zhao, "A CPW-fed dual-band MIMO antenna with enhanced isolationfor 5G application," *Progress In Electromagnetics Research M*, Vol. 98, 11–20, 2020.
18. Kumar, A., A. Q. Ansari, B. K. Kanaujia, and J. Kishor, "High isolation compact four-port MIMO antenna loaded with CSRR for multiband applications," *Frequenz*, Vol. 72, No. 9–10, 415–427, 2018.
19. Garg, R., P. Bhartia, I. Bahl, and A. Ittipiboon, *Microstrip Antenna Design Handbook*, Artech House Inc., 2001.
20. Hasan, M. I., M. A. Motin, and M. S. Habib, "Circular ring slotting technique of making compact microstrip rectangular patch antenna for four band applications," *2013 International Conference on Informatics, Electronics and Vision (ICIEV)*, 1–4, Dhaka, 2013.